Membrane-Bound Orientation and Position of the Synaptotagmin I C2A Domain by Site-Directed Spin Labeling†

April A. Frazier,‡ Christina R. Roller,‡ Jessica J. Havelka,§ Anne Hinderliter,§ and David S. Cafiso*,‡

Department of Chemistry and Biophysics Program at the University of Virginia, Charlottesville, Virginia 22904-4319, and Department of Pharmaceutical Sciences at North Dakota State University, Fargo, North Dakota

Received September 7, 2002; Revised Manuscript Received November 10, 2002

ABSTRACT: Site-directed spin labeling was used to determine the membrane orientation and insertion of the C2A domain from synaptotagmin I. A series of single cysteine mutants of the C2A domain of synaptotagmin I was prepared and labeled with a sulfhydryl specific spin label. Upon Ca^{2+} or membrane binding, the EPR line shapes of these mutants reveal dramatic decreases in label mobility within the Ca^{2+}-binding loops. This loss in mobility is likely due in part to a reduction in local backbone fluctuations within the loop regions. Power saturation was then used to determine the position of each spin-labeled site along the bilayer normal, and these EPR distance constraints were used along with the high-resolution solution structure of C2A to generate a model for the orientation and position of the domain at the membrane interface. This model places the polypeptide backbone of both the first and third Ca^{2+}-binding loops in contact with the membrane interface, with several labeled side chains lying within the bilayer interior. All three Ca^{2+}-binding sites lie near a plane defined by the lipid phosphates. This model indicates that there is some desolvation of this domain upon binding and that hydrophobic as well as electrostatic interactions contribute to the binding of C2A. When compared to the C2 domain from cPLA2 (Frazier et al. (2002) *Biochemistry 41*, 6282), a similar orientation for the β-sandwich region is found; however, the cPLA2 C2 domain is translocated 5−7 Å deeper into the membrane hydrocarbon. This difference in depth is consistent with previous biophysical data and with the difference that long-range electrostatic interactions and desolvation are expected to make to the binding of these two C2 domains.

The reversible association of key cytoplasmic proteins to the membrane interface is of critical importance for much of the biochemistry that takes place during cell signaling. Proteins may be targeted to membrane surfaces by a number of mechanisms, including protein acylation or long-range Coulombic interactions between highly basic protein motifs and negatively charged membrane interfaces (*2*, *3*). Cytoplasmic proteins are also targeted to membranes by specific protein domains, which interact either with particular lipids or bind nonspecifically to the membrane interface (*4*). These membrane binding domains are widely distributed in proteins that function in cell signaling, and they include pleckstrin homology (PH),[1] C2, FYVE, Phox, and ENTH domains (*5*−*11*). Many PH domains interact with specific lipids such as $PI(4,5)P_2$; however, others appear to interact weakly or nonspecifically with the membrane interface (*12*, *13*). FYVE, Phox, and ENTH domains also have the capacity to interact with specific polyphosphoinositides. C2 domains usually mediate Ca^{2+}-dependent membrane attachment, although some C2 domains constitutively bind membranes and are not Ca^{2+}-dependent (*14*).

The C2 domain was originally identified as one of four distinct conserved domains in Ca^{2+}-dependent isoforms of PKC, but it has now been identified in over 100 proteins that function in a range of cell signaling events (*15*−*17*). Synaptotagmin is a membrane protein that appears to serve as a Ca^{2+} sensor for regulated exocytosis in neurons (*18*), and it possesses two C2 domains that are tied together by a flexible linker. In the presence of Ca^{2+}, the first C2 domain (C2A) binds strongly to membranes containing negatively charged lipids, but it has low affinity for membranes lacking acidic lipids (*19*, *20*). The role of the second C2 domain (C2B) in synaptotagmin is less clear. It has been reported to function in both Ca^{2+}-dependent membrane and protein binding (*21*), and recent reports indicate that Ca^{2+}-binding to this domain may be critical for membrane fusion (*22*).

† This work was supported by NIH Grant GM62305 (D.S.C.), NSF Grant EPS-9874802 (A.H.), and NSF Grant OSR-9452892 (J.J.H.) (AURA Award).

* Corresponding author. E-mail: cafiso@virginia.edu. Tel: 434-924-3067.

‡ University of Virginia.

§ North Dakota State University.

[1] Abbreviations: bR, bacteriorhodopsin; AEBSF, aminoethylbenzene sulfonyl fluoride hydrochloride; CBL, Ca^{2+}-binding loop; DPPH, α,α′-diphenyl-β-picrylhydrazyl; ENTH, epsin N-terminal homology; EPR, electron paramagnetic resonance spectroscopy; HEPES, *N*-2-hydroxyethylpiperazine-*N*′-2-ethanesulfonic acid; LUV, large unilamellar vesicle; MTSSL, methanethiosulfonate spin label; NiEDDA, nickel(II) ethylenediaminediacetic acid; $PI(4,5)P_2$, phosphatidylinositol 4,5-bisphosphate; PH, pleckstrin homology; PMSF, phenylmethanesulfonyl fluoride; PKC, protein kinase C; PLC-δ, phospholipase C; cPLA2, cytosolic phospholipase A_2-α; PC, phosphatidylcholine; POPC, palmitoyloleoylphosphatidylcholine; POPS, palmitoyloleoylphosphatidylserine; PS, phosphatidylserine; SDSL, site-directed spin labeling; synIC2A, synaptotagmin I C2A domain; SUV, small unilamellar vesicle.

10.1021/bi0268145 CCC: $25.00
Published on Web 12/12/2002

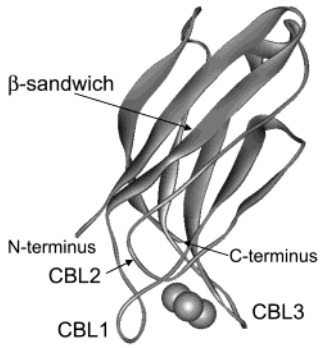

FIGURE 1: NMR-derived solution structure of the synaptotagmin I C2A domain (PDB code 1BYN) showing the eight-stranded β-sandwich region, three Ca^{2+}-binding loops (CBL), and three bound Ca^{2+} ions (*36*).

Figure 1 shows a solution structure for the synaptotagmin I C2A domain (synIC2A) (*23*). All C2 domains examined thus far have a similar fold and consist of an eight strand β-sandwich formed from two 4-stranded β-sheets. The loops that connect the β-strands on one end of the domain form binding sites for three Ca^{2+} ions, and it is these loops that interact with the membrane interface. Information on the docking and orientation of C2 domains on membrane surfaces has been obtained using several approaches. For example, NMR spectroscopy has been used to identify the membrane-interacting face of C2 domains from chemical shift changes that take place in the presence of micelles (*24*, *25*); however, chemical shift changes at regions distal to the putative binding loops have been observed. For the C2 domain from cytosolic phospholipase A2 (cPLA2), fluorescence and EPR spectroscopy have provided information on membrane docking (*26*−*28*). These results clearly indicate that the domain from cPLA2, which does not require acidic lipid for binding, penetrates deeply into the membrane interior. This finding is also consistent with the results of photolabeling experiments and monolayer surface pressure measurements (*26*, *29*, *30*). In contrast, the synaptotagmin C2A domain is thought to associate peripherally with the bilayer (*16*, *20*), although fluorescence labeling indicates that at least two residues penetrate the bilayer (*31*). For most C2 domains, precise information on their membrane orientation and depth of penetration that could be used to determine the nature of the intermolecular contacts between the protein and membrane is not generally available.

A number of different mechanisms have been proposed to account for the Ca^{2+}-dependent binding of C2 domains. For example, Ca^{2+}-binding affinity increases dramatically in the presence of lipid (*32*, *33*), indicating that Ca^{2+} coordinates both phospholipid and residues from the C2 domain (*23*, *34*). Ca^{2+} has also been proposed to induce conformational changes, which exposes residues that interact hydrophobically with the membrane or create binding sites for lipids (*35*). Electrostatic interactions likely play a major role in the membrane association of the C2A domain from synaptotagmin (*36*) and may have an important role in regulating the Ca^{2+}-dependent membrane attachment of C2 domains. Recent computational work indicates that Ca^{2+} makes at least two contributions to the binding of C2 domains (*37*). First, it enhances the positive electrostatic potential on the membrane binding surface of the domain, thereby increasing the Coulombic attraction to negatively charged membrane surfaces. Second, Ca^{2+}-binding reduces the desolvation energy of the C2 domain on its membrane binding face. The importance of these two effects is thought to be different for different C2 domains. In the case of the C2 domain from cPLA2, which preferentially binds to neutral zwitterionic phosphatidylcholine (PC) membranes, Ca^{2+}-binding appears to act by reducing the desolvation energy. However, for the C2A domain from synaptotagmin, which requires acidic lipids such as phosphatidylserine (PS) for membrane binding, Ca^{2+} is thought to modulate the long-range Coulombic interaction between the domain and the negatively charged membrane surface.

Scheme 1

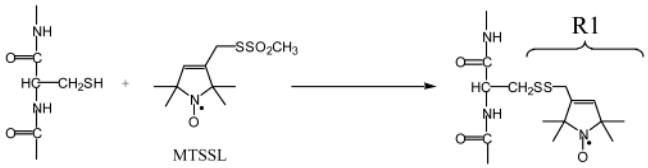

Recently, site-directed spin labeling (SDSL) was used to determine the membrane penetration and orientation of the C2 domain from cPLA2 on the membrane interface (*28*). This approach made use of a series of single cysteine mutants that were derivatized with a methane thiosulfonate spin label (MTSSL). This chemistry incorporates the spin-labeled side chain, R1 (Scheme 1), in place of the native side chain (*38*−*41*). EPR spectroscopy was then used to determine the positions of the labeled side-chains along the bilayer normal, and the positions were used to generate a model for the membrane bound domain. This work indicated that the cPLA2 C2 domain penetrates the membrane interface so that the Ca^{2+}-binding sites lie several Å below the membrane interface. Side chains from the Ca^{2+}-binding loops penetrate as much as 15 Å below the level of the lipid phosphates. In this model a major portion of the domain is dehydrated upon membrane binding, consistent with the predictions of recent electrostatic calculations (*37*).

In the present work, we use site-directed spin labeling to examine the membrane binding of the C2A domain from synaptotagmin I, and we generate a model for the orientation and depth of penetration of the domain on membranes containing acidic lipid. Although this domain is believed to interact electrostatically, our data demonstrate that portions of this domain do penetrate the bilayer; however, the domain does not assume as deep a position in the bilayer as does the C2 domain from cPLA2. Our EPR data also reveal decreases in synIC2A dynamics upon Ca^{2+} and membrane binding. The interpretation of these results in light of computational work and other experimental work is discussed.

MATERIALS AND METHODS

Materials. 1-Palmitoyl-2-oleoyl-*sn*-glycero-3-phosphocholine (POPC) and 1-palmitoyl-2-oleoyl-*sn*-glycero-3-phosphoserine (POPS) were from Avanti Polar Lipids, Inc. (Birmingham, AL). All lipids were greater than 99% pure, as determined by chromatography on Adsorbosil-Plus thin-layer chromatography plates (Alltech Associates, Inc., Deerfield, IL). The sulfhydryl reactive spin label, (1-oxyl-2,2,5,5-tetramethyl-Δ^3-pyrroline-3-methyl) methanethiosulfonate (MTSSL), was purchased from Toronto Research

Chemicals, Inc. (North Fork, Ontario, Canada). The paramagnetic reagent, nickel(II)-ethylenediamine-N,N′-diacetic acid (NiEDDA), was synthesized as described previously (*42*). GSTrap FF pre-packed columns, benzamidine pre-packed columns, HiPrep desalting column, and thrombin protease were purchased from Amersham Biosciences (Piscataway, NJ). High-fidelity Vent DNA polymerase and all restriction endonucleases were obtained from New England Biolabs (Beverly, MA).

Buffers. PBS (phosphate buffered saline): 10 mM Na_2HPO_4, 2.7 mM KCl, 1.8 mM KH_2PO_4, 140 mM NaCl, pH 7.3. Resuspension buffer: PBS, 1 mM DTT, 5 mM EGTA, 1% protease inhibitors (AEBSF or PMSF, leupeptin, aprotinin), and 2% Triton X-100. Wash buffer: 750 mM NaCl, 25 mM EGTA, 50 mM Tris, pH 8.4. Calcium buffer: 1 mM $CaCl_2$, 100 mM NaCl, 20 mM HEPES, pH 7.4. Ficoll calcium buffer: calcium buffer in 20% Ficoll 400. Ficoll EDTA buffer: 5 mM EDTA, 20 mM HEPES, 100 mM NaCl, pH 7.4, and 20% Ficoll 400.

DNA Modification. Dr. Carl Creutz (Department of Pharmacology, University of Virginia) generously provided DNA of synIC2A, in the vector pGEX-KG (*43*), encoding amino acid residues 96−265. The plasmid encoding the GST-fusion protein containing wild-type synIC2A has been described previously (*44*). All DNA modifications followed published protocols (*45*), and the two-step polymerase chain reaction (PCR) was used to produce 19 single-cysteine mutants of C2A. Individual cysteine residues were introduced at positions, 142, 170, 171, 173−176, 197, 199, 201, 202, 229, 231, 233, 234, 236, 237, 239, and 240. All cysteine substitutions were confirmed by DNA sequencing.

Protein Purification. The mutant plasmids for synIC2A were transformed into BL21(DE3)pLys*S* cells. A single colony was used to inoculate a 100 mL pre-culture of Luria-Bertani (LB) media containing 50 mg/L ampicillin, and the pre-culture was grown overnight at 37 °C, shaking vigorously, in a baffled flask. A 1 L culture of LB media in a 2.8L Fernbach flask, with 50 mg/L ampicillin, was inoculated with the pre-culture and grown to an OD_{595} of 0.8. Expression was induced by addition of 0.1 mM isopropyl-β-D-thiogalactopyranoside and proceeded for 4−6 h at 20 °C, shaking vigorously. Bacteria were collected by centrifugation at 10 000 rpm for 30 min at 4 °C, and the resulting bacterial pellet was solubilized in Resuspension Buffer. The cells were lysed while on ice with a micro-probe tip sonicator, or with a French Press. After disruption, the lysate was repeatedly passed through a Dounce homogenizer before centrifugation at 14 000 rpm for 30 min at 4 °C. The clarified supernatant was preserved at 4 °C, for up to 3 months and, if required, filtered with a 0.45 μm syringe filter.

The synIC2A−GST fusion protein from the clarified supernatant was purified by affinity chromatography on GSTrap FF pre-packed columns using an AKTA Prime system (Amersham Biosciences, Piscataway, NJ). Purified synIC2A was cleaved from the column with thrombin, eluted with Wash Buffer, concentrated using 10 000 MWCO centripreps (Millipore, Bedford, MA), buffer exchanged into 0.5 mM ammonium bicarbonate, and lyophilized. Protein purity and identity were confirmed by SDS−PAGE (Bio-Rad, Hercules, CA) and mass spectrometry (Scripps Center for Mass Spectrometry, La Jolla, CA). The molecular weight for synIC2A was approximately 21.5 kDa, consisting of synaptotagmin residues 96−265 plus 25 additional residues from the pGEX vector. In some preparations, gel electrophoresis and mass spectrometry identified an additional 19 kDa protein. As noted previously, synaptotagmin I contains a hypersensitive proteolytic cleavage site, which is thought to be located between residues 90−110 (*33*, *46*). The 19 kDa protein was confirmed by Edman sequencing to be a shortened version of C2A, where the hypersensitive proteolytic site is located between residues 104 and 105.

Spin Labeling C2A Protein. Lyophilized protein was brought up in 1.75 mL of Spin Labeling Buffer (PBS and 5 mM EGTA). DTT was added at a mole ratio of 3:1 DTT:protein, and MTSSL was subsequently added in a mole ratio of 10:1 MTSSL:DTT. The mixture was thoroughly shaken and stored in the dark at room temperature for 2−12 h. Excess spin label was removed by desalting on a HiPrep 16/10 column. At the same time, the spin-labeled protein was buffer exchanged into Calcium Buffer. Sequentially concentrating with centripreps and centricons yielded stock protein concentrations of 0.3−2 mM, as determined using a Bradford Assay (Pierce, Rockford, IL).

Large Unilamellar Vesicles. Large unilamellar vesicles (LUVs) were prepared with a POPC:POPS ratio of 3:1 by mixing the appropriate aliquots of lipids, drying the solution under a stream of argon, and vacuum desiccating the mixture overnight. The resulting film was hydrated in half the volume required with a buffer of 100 mM NaCl, 50 mM HEPES, pH 7.4, for 1 h, vortexed thoroughly, and extruded through a polycarbonate filter with a 0.1 μm pore diameter using a hand-held Mini-Extruder (Avanti Polar Lipids, Birmingham, AL). After extrusion, the remaining buffer was added and consisted of 2 mM $CaCl_2$, 100 mM NaCl, and 50 mM HEPES, pH 7.4. The final calcium ion concentration was 1 mM. Lipids were extruded at a total concentration of 80 or 150 mM and then diluted for use.

Measurement of C2A Domain Membrane Affinities. Cation affinities of the spin-labeled C2A domain mutants in the presence of membranes were measured with a Tb^{3+} fluorescence binding assay as described previously (*47*) using either an SLM Aminco 8100 or a Jobin Yvon-Spex Fluorolog-3 model FL3-11 fluorimeter and a Teflon-capped 300 μL mini-fluorimeter cell (McCarthy Scientific, Fullerton, CA). The tryptophan on synIC2A was excited at a wavelength of 295 nm, and fluorescence intensities were monitored at wavelengths of 342 nm (Trp) and 545 nm (Tb^{3+}). The intensity at 342 nm was used to calculate the binding affinity as it displayed the larger change upon Tb^{3+} binding. Spectra were collected after allowing an incubation time of 15 min to achieve equilibrium, and the samples were continuously stirred throughout the experiment.

EPR Measurements. Protein sample concentrations for EPR spectroscopy typically ranged from 20 to 300 μM, and the lipid vesicles (LUVs) were used at a concentration of 20 mM or higher to ensure complete membrane binding and low surface densities. EPR spectra were recorded using a Varian E-line Centuries series spectrometer fitted with a microwave preamplifier and an X-band loop-gap resonator (Medical Advances, Milwaukee, WI). Spectra were recorded at room temperature and were typically an average of twenty-five 30 s scans. From the peak-to-peak line width of the EPR central resonance, δ, the scaled mobility, M_s, for the nitroxide was determined from: $M_s = (\delta^{-1} - \delta_i^{-1})/(\delta_m^{-1} - \delta_i^{-1})$. Here

δ_m and δ_i represent the line widths of the most mobile and least mobile R1 side chains previously observed in proteins (*48*).

Continuous-wave power saturation measurements were performed as described previously (*58*). Due to steric constraints and purification problems, residues 197R1 and 199R1 were not included in the power saturation data set. From these experiments, a collision parameter for O_2 (Π^{oxy}) and a collision parameter for NiEDDA (Π^{NiEDDA}) were determined. A depth parameter, Φ, was then calculated using the following expression:

$$\Phi = \ln\left[\frac{\Pi^{oxy}}{\Pi^{NiEDDA}}\right] \quad (1)$$

Modeling the Orientation of the synIC2A Domain. The orientation of the synaptotagmin I C2A domain was modeled as described previously (*28*) by obtaining the best fit of protein orientation and depth to the high-resolution solution structure of the domain, known depth calibration points, and an empirical form for the depth parameter Φ. In short, the R1 side chain was appended to the NMR-derived structure of synIC2A (PDB code 1BYN) at the labeled sites. The labels were placed in configurations determined by recent crystallographic studies on R1 (*49*), where the first, second, and third dihedral angles are in a *g*+, *g*+, *g*− conformation. The exceptions were residues 199 and 239 (*g*+, *g*+, *g*+), residues 202 and 237 (*g*+, *t*, *g*−), and residue 197 (*g*+, *t*, *g*+) due to steric constraints. A set of coordinates for the nitrogen atoms on the R1 side chain was then generated. A model for the membrane bound position of synIC2A at the interface was defined by three Euler angles and its position along the bilayer normal.

As discussed previously (*28*), the depth parameter is assumed to have the following behavior:

$$\Phi = A \tanh[B(x - C)] + D \quad (2)$$

where x represents the distance of the label from the lipid phosphates (positive values of x are inside and negative values are outside the bilayer), A and D set the bulk values of Φ in water and hydrocarbon, C determines the position of the inflection point of the curve, and B determines the slope of the curve. The position and orientation of the domain was varied along with the quantities ($D - A$), B, and C of eq 2 to find the best fit between the synIC2A domain data, the spin-labeled phosphatidylcholine (PC) and bacteriorhodopsin (bR) calibration points, and the form of eq 2. The data from doxyl-labeled PC and spin-labeled bacteriorhodopsin mutants were obtained previously for membranes having the same lipid composition as that used here (*28*). The resulting model is constrained by the form of eq 2, Φ data for synIC2A, Φ values for spin-labeled lipids and bR, the allowed configurations for the R1 side chain, and geometrical constraints imposed by the solution structure of the synIC2A domain.

RESULTS

Membrane Binding of Wild-Type and Single Cysteine synIC2A Mutants. For each of the spin-labeled synIC2A mutants, membrane binding was determined and compared to wild-type protein by monitoring terbium affinity to synIC2A in the presence of membranes (see methods). This was carried out to ensure that each mutant C2A was folded correctly and retained its membrane binding function. The cation dissociation constant, K_d, for wild-type synIC2A was found to be 8 ± 2 μM in the presence of 75:25 POPC:POPS LUVs. This is consistent with the K_d value expected for Tb^{3+} based upon the K_d value found previously for Ca^{2+} (*16*). Table 1 summarizes the affinities measured for the spin-labeled synIC2A mutants in the presence of membranes. Compared to the wild-type value, the membrane binding affinity is not significantly altered by introducing the spin-labeled side chain into the synIC2A domain. The values determined for the cation-dependent membrane binding do not vary by more than a factor of ≈2 and therefore represent relatively small changes in the free energy of binding. As expected, the biggest changes are seen when the R1 side chain is substituted for membrane-interacting residues on loop 1 and basic residues that presumably interact with acidic lipids upon binding. This result indicates that this domain is folded correctly and that the incorporation of these labels does not significantly alter its membrane binding properties. This is consistent with a previous site-directed spin labeling study on the C2 domain from cPLA2, which demonstrated that the incorporation of spin labels onto the exterior surface of the domain had little effect on Ca^{2+}-dependent protein binding (*28*).

Table 1: Tb^{3+} Binding Constants to C2A in the Presence of POPC:POPS Vesicles[a]

mutant	K_D lipid/ μM	mutant	K_D lipid/ μM	mutant	K_D lipid/ μM
WT	8 ± 2	T176R1	16 ± 3	R233R1	17 ± 3
L142R1	8 ± 2	V197R1	4 ± 1	*F*234R1	4 ± 1
A170R1	7 ± 1	R199R1	8 ± 2	K236R1	13 ± 3
L171R1	12 ± 2	T201R1	6 ± 1	H237R1	5 ± 1
M173R1	7 ± 1	L202R1	4 ± 1	*I*239R1	5 ± 1
G174R1	8 ± 2	Y229R1	8 ± 2	I240R1	5 ± 1
G175R1	14 ± 3	F231R1	8 ± 2		

[a] As described previously (*47*), these binding constants represent the Tb^{3+}-dependent membrane binding affinities for the synIC2A domain. The errors shown in the table are based on instrumental and sample reproducibility and are approximately 20% of the measured values.

EPR Spectra Reveal Secondary Structure and Membrane Insertion. The EPR spectra for synIC2A in aqueous solution and bound to POPC:POPS bilayers are shown in Figure 2. In the absence of lipid, there is considerable variation in the EPR line shapes. Several spectra (142R1, 197R1, 229R1, 239R1, and 240R1) are quite broad and correspond to spectra that might arise from spin labels with effective isotropic correlation times on the order of 4−5 ns (*50*). These broader EPR resonances result from labels that are placed within the β-sandwich region of synIC2A. A number of spectra (173R1, 174R1, 201R1, 233R1, and 236R1) are much narrower and arise from nitroxides having effective isotropic correlation times in the 1.5−2 ns range. This time scale is somewhat shorter than the correlation time expected for overall rotational diffusion of the protein, which is approximately 6 ns according to the Stoke−Einstein equation. These narrower spectra all arise from labels placed within loop regions of synIC2A, and the additional narrowing likely arises from local or backbone motional averaging of the nitroxide magnetic interactions.

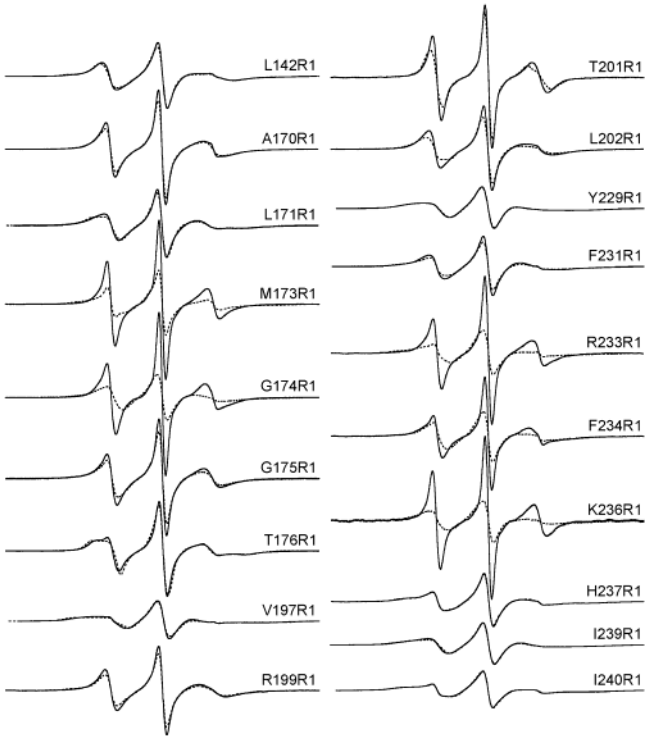

FIGURE 2: EPR spectra of 19 R1 mutants of synIC2A in aqueous solution (solid lines) and bound to lipid vesicles (dashed lines) composed of POPC:POPS (3:1). All the spectra are 100 G scans and are normalized against their second integrals. Direct comparison of the EPR amplitudes provides an approximate measure of the extent of motional averaging of the spin label (Figure 3B).

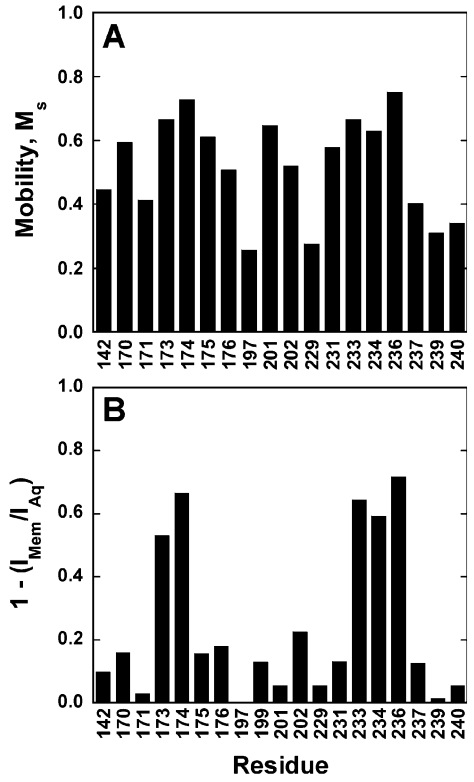

FIGURE 3: (A) Scaled mobilities for the spin-labeled synIC2A in Ficoll Calcium Buffer, calculated using $\delta_i = 8.4$ G and $\delta_m = 2.1$ G (*48*). High-viscosity solutions reduce the tumbling rate of the protein without altering the rate of side chain motion (*51*). As a result, the spectra and M_s values are only affected by motional averaging at the labeled site. (B) Normalized peak-to-peak amplitudes of the central resonance ($m_I = 0$) comparing aqueous and membrane bound signals. I_{mem} and I_{aq} represent the normalized amplitudes for the synIC2A domain spectra in the presence of membranes or in aqueous solution, respectively. The amplitudes are scaled on the *y*-axis so that a value of 0 represents no change in amplitude, while a value of 1 represents a complete loss of signal upon binding.

A more quantitative comparison of the differences in line shapes is shown in Figure 3A, which compares the values for the scaled mobilities, M_s, for each of the labeled sites in ficoll calcium buffer. The value of M_s provides a qualitative measure of R1 motion, where values of 1 and 0 represent the most mobile and least mobile spin-labeled side chains seen in proteins (*38*). For side chains that are not in tertiary contact, the value of M_s is expected to be directly correlated with the dynamics of the protein backbone (*48*). It is readily apparent that the largest values of M_s (173R1, 174R1, 175R1, 201R1, 233R1, 234R1 and 236R1) arise from spin labels placed within loop regions of the protein, indicating that these are the most mobile regions of synIC2A in solution. The lowest values of M_s (197R1, 229R1, 239R1 and 240R1) arise from labels attached to the β-fold of the protein. Thus, the EPR spectra, as observed previously (*51*), generally reflect the secondary structure into which the label is incorporated.

All the synIC2A domain mutants undergo at least a slight broadening or decrease in normalized amplitude upon membrane binding (see Figure 2), which is expected since the overall rotational motion in solution can no longer contribute to the motional averaging of the nitroxide interactions. However, several spectra (173R1, 174R1, 233R1, 234R1, and 236R1) exhibit a much more dramatic decrease in amplitude upon membrane binding, indicating a significant loss of R1 motion at these sites. Figure 3B shows the changes in normalized EPR amplitude for the labeled sites upon membrane binding. The largest changes occur for those sites on Ca^{2+}-binding loops 1 and 3; however, large changes in amplitude are not seen for residues in loop 2. As shown below, loops 1 and 3 penetrate the bilayer whereas loop 2 does not; hence, these changes in nitroxide motion appear to distinguish sites that are within the lipid bilayer for membrane bound synIC2A. The change in motional averaging upon binding could arise from two effects. First, the bilayer environment might alter the local side chain motion of R1; or second, the membrane environment might reduce the amplitudes or rates of local backbone fluctuations (*1*).

Ca^{2+} Removal Alters the Backbone Dynamics of the Membrane Binding Loops. Shown in Figure 4 are the EPR spectra for synIC2A in high-viscosity solution in the presence and absence of Ca^{2+}. In this high-viscosity solution, protein rotational diffusion makes little contribution to the EPR line shapes (*51*), and the EPR spectra are defined by the local label motion and local backbone fluctuations (*48*). At many sites, the EPR spectra are identical or quite similar in the presence and absence of Ca^{2+}; however, at several sites within the loop regions, dramatic increases in label mobility are indicated when Ca^{2+} is removed (for example, sites 173−176). Because Ca^{2+} binding does not alter the structure of synIC2A (*36*), these differences do not result from changes in tertiary contact. Furthermore, evidence for strong tertiary contact of the spin label (large hyperfine extrema) is not seen in most of these EPR spectra. Recent work on the motional averaging of the R1 side chain suggests that the changes

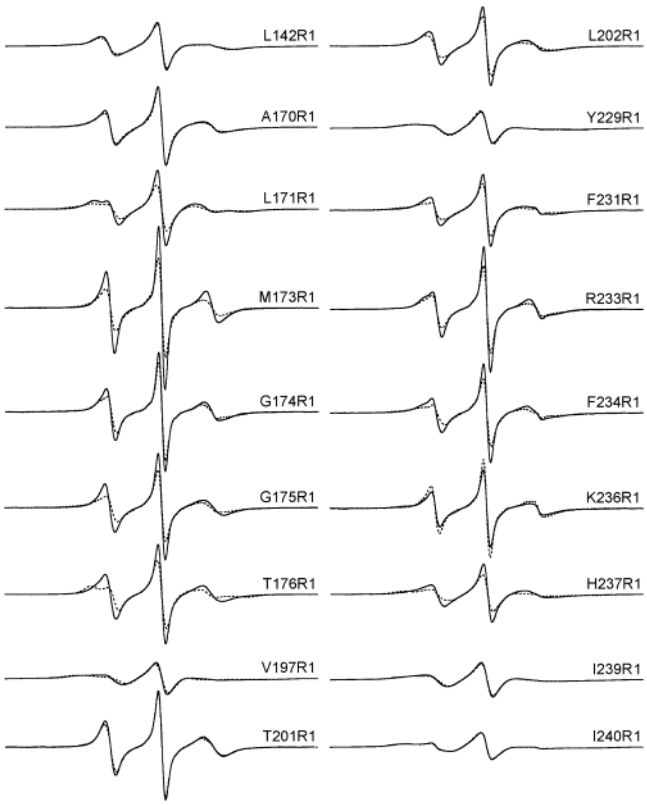

FIGURE 4: EPR spectra in high viscosity solution (20% Ficoll 400) in the presence (dashed lines) and absence (solid lines) of Ca^{2+}. Ca^{2+} was removed by placing the protein into Ficoll EDTA Buffer. The spectra are 100 G scans and are normalized against their second integrals.

seen in Figure 4 upon Ca^{2+} removal are the result of changes in backbone dynamics (*48*) and that the data indicate increased rates and/or amplitudes of backbone fluctuations, particularly in loop 1, upon Ca^{2+} removal.

To provide a more meaningful interpretation of these Ca^{2+} changes, several spectra shown in Figure 4 were simulated with the microscopic-order-macroscopic-disorder model described previously (*52*), using the X_4/X_5 model for R1 side-chain motion (*1*).[2] For T176R1 in the presence of Ca^{2+}, the spectrum can be approximated by $\tau_c = 1.05$ ns and $S = 0.5$, where τ_c is the rotational correlation time and S defines a simple axially symmetric restoring potential used in the simulation (S is defined as: $S = -1/2(3\cos 2\theta - 1)$, where θ is the average angle between the protein fixed director and the z-axis of the diffusion tensor). When Ca^{2+} is removed, the spectrum is approximated by $\tau_c = 1.05$ ns and $S = 0.25$. This difference in S suggests that there is a substantial decrease in ordering of the nitroxide upon Ca^{2+} removal; for example, the decrease in order could be produced by an increase in backbone rocking motion of approximately 8°.

[2] The magnetic parameters and model for motion used in this simulation are described in detail elsewhere (*1*). The diffusion tilt angles used were $\beta_D = 36.2°$ and $\alpha_D = 4.0°$. It should be noted that these parameters have been derived only for exposed helical sites; nonetheless, they work well to approximate the EPR spectra on at least some Ca^{2+}-binding loop sites. In a helix, the likely orientation for the p-orbital of the nitroxide on R1 makes it particularly sensitive to backbone rocking motions; however, at this time we do not know its orientation on loop sites and cannot rigorously assign the decrease in order to a specific backbone motion.

Table 2: Collision and Depth Parameters for Spin-Labeled C2A Domain Mutants[a]

mutants	Π^{oxy}	Π^{NiEDDA}	Φ	distance model[b]	distance curve[c]
L142R1	0.16[d]	1.1[e]	−1.9	−10.6	−6.0
A170R1	0.31	3.0	−2.3	−7.2	(−19.1)
L171R1	0.22	1.2	−1.7	−9.6	−3.9
M173R1	0.42	1.7	−1.4	−3.4	−1.7
G174R1	0.50	0.34	+0.4	5.3	5.8
G175R1	0.38	2.3	−1.8	−1.1	−4.9
T176R1	0.37	2.6	−1.9	−6.5	−6.0
T201R1	0.28	1.9	−1.9	−7.6	−6.0
L202R1	0.29	3.2	−2.4	−10.1	- - - -
Y229R1	0.25	1.9	−2.0	−13.3	(−7.5)
F231R1	0.23	1.3	−1.7	−3.8	−3.9
R233R1	0.39	1.6	−1.4	−0.3	−1.7
F234R1	0.46	0.25	+0.6	5.1	6.4
K236R1	0.38	0.69	−0.6	1.4	2.3
H237R1	0.26	2.0	−2.0	−0.7	(−7.5)
I239R1	0.17	1.4	−2.1	−8.0	(−9.4)
I240R1	0.22	1.3	−1.8	−6.1	−4.9

[a] Collision data for the C2A domain is given bound to PC:PS LUVs. [b] Distances for the C2 domain spin labels were obtained from the model shown in Figure 6 and correspond to the position of the nitrogen atom on R1 in angstroms from the plane of the lipid phosphates. Positive distances are within the bilayer; negative distances are in the aqueous phase. The uncertainty in these distances, as defined by the uncertainty in Φ and constrained by the structural model, is on the order of ±3 Å. [c] Distances were calculated from the experimental values of Φ using eq 2. Parentheses indicate values of $\Phi < -1.9$, which are obtained for sites lying in the aqueous phase greater than a few Å from the membrane. For these sites, distances are poorly determined as indicated by eq 2 and Figure 5. [d] The uncertainty in the Π^{oxy} value is on the order of ±0.05. [e] The uncertainty in Π^{NiEDDA} is on the order of ±0.4.

Power Saturation Parameters Indicate that Loops 1 and 3 Insert into the Bilayer. As described above (see Methods), 17 spin-labeled derivatives of the syn1C2A domain were power-saturated to generate collision parameters between the R1 side chain and either oxygen or NiEDDA. Table 2 summarizes the Π values and the corresponding values of the depth parameter, Φ, calculated according to eq 1.

Previous work has shown that Φ values more negative than −2 are associated with sites that are in the bulk aqueous phase, lying at distances greater than 5 Å from the level of the lipid phosphates (*28*). As seen in Table 2, five labeled sites have values of Φ that are less than or equal to −2.0. At these sites, lower values of $\Pi^{\circ xy}$ and higher values of Π^{NiEDDA} are observed, consistent with their placement in the bulk aqueous phase. The data in Table 2 lists 12 spin-labeled sites on membrane bound synIC2A with Φ values greater than −2, indicating that these sites reside close to or within the membrane bilayer. R1 side chains in loop 1 (G174) and loop 3 (*F*234 and K236) have the largest Φ values, indicating that sites in loops 1 and 3 are inserted into the membrane bilayer. Labels on loop 2 (T201 and L202) reveal relatively low Φ values and suggest that loop 2 does not interact with the membrane.

Modeling the Orientation of the Membrane-Bound synIC2A Domain. Using the depth data shown in Table 2 and the solution structure of synIC2A, the Euler angles and position along the bilayer normal for the synIC2A domain were varied until a best fit was obtained with lipid and protein calibration data and the form of eq 2 (see Methods). This fit is shown in Figure 5, where the *x*-axis represents the modeled distance from the lipid phosphates, and the *y*-axis displays the

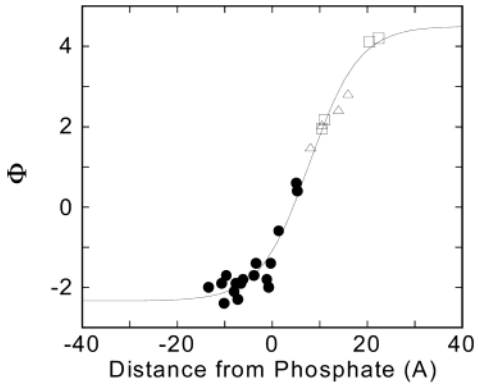

FIGURE 5: Depth calibration curve showing the fit of eq 2 and the dependence of Φ on position from the lipid phosphates. The *y*-axis values (Φ) for the synIC2A data (●) are experimentally determined values (Table 2), and the *x*-axis values (distances) are generated from the high-resolution solution structure of synIC2A in its best fit position and orientation. Calibration points generated previously (*28*) from bacteriorhodopsin (□) and doxyl spin-labeled lipids (△ are also shown and were used in the fit (see Methods).

experimental Φ values. The solid line represents the depth dependence for Φ, defined by eq 2, that best fits the data. For this fit, the bulk hydrophobic limit was fixed at a value of $\Phi = 4.5$. The bulk aqueous value of Φ was allowed to vary, and the fit to the data yielded an aqueous limit of $\Phi = -2.3$. This value is close to the average aqueous value of Φ obtained for the cPLA2 C2 domain ($\Phi = -2.5$) (*28*), and it is close to the experimentally determined aqueous value of Φ for 3-carboxyproxyl ($\Phi = -2.6$). The best fit parameters obtained for eq 2 were 3.4, 0.1, 7.9, and 1.1 for A, B, C and D, respectively, and are very close to the values derived from data for the cPLA2 C2 domain (*28*).

The depth dependence for Φ generated from the synIC2A mutants indicates that Φ reaches 95% of its bulk aqueous value at a distance of 5 Å from the membrane interface consistent with previous findings (*28*). In addition, the best fit model indicates that labels with values of Φ greater than −1.1 are inserted into the bilayer. While there is scatter among the most negative depth parameters, the data is fit reasonably well by eq 2 and suggests that large structural changes do not take place in the synIC2A domain upon membrane binding. The measurements of Φ are quite reproducible; however, the uncertainty in the conformation of the R1 side chain represents a significant source of error. While the first two dihedral angles for R1 are relatively well defined, the third dihedral angle may have orientations of either +90° or −90° (*1*, *49*); in addition, rotation about X_4 adds a distance variation of approximately 3 Å. When the spin labels are directed either toward or away from the bilayer (within the constraints discussed previously (*49*)), $X_3 = +90°$ provides the best fit. As discussed previously, other sources of error include the exact form for eq 2 and in the membrane bound conformation of synIC2A (*28*).

Figure 6A shows the orientation and position of the synaptotagmin C2A domain at the POPC:POPS interface that is obtained from the fit in Figure 5. In this orientation, side chains from both loops 1 and 3 are inserted into the bilayer with the backbone of loop 3 inserted approximately 5 Å below the level of the phosphates. The backbone of loop 1 is positioned so that it resides close to the level of the lipid phosphates. Neither the side chains nor the backbone of loop

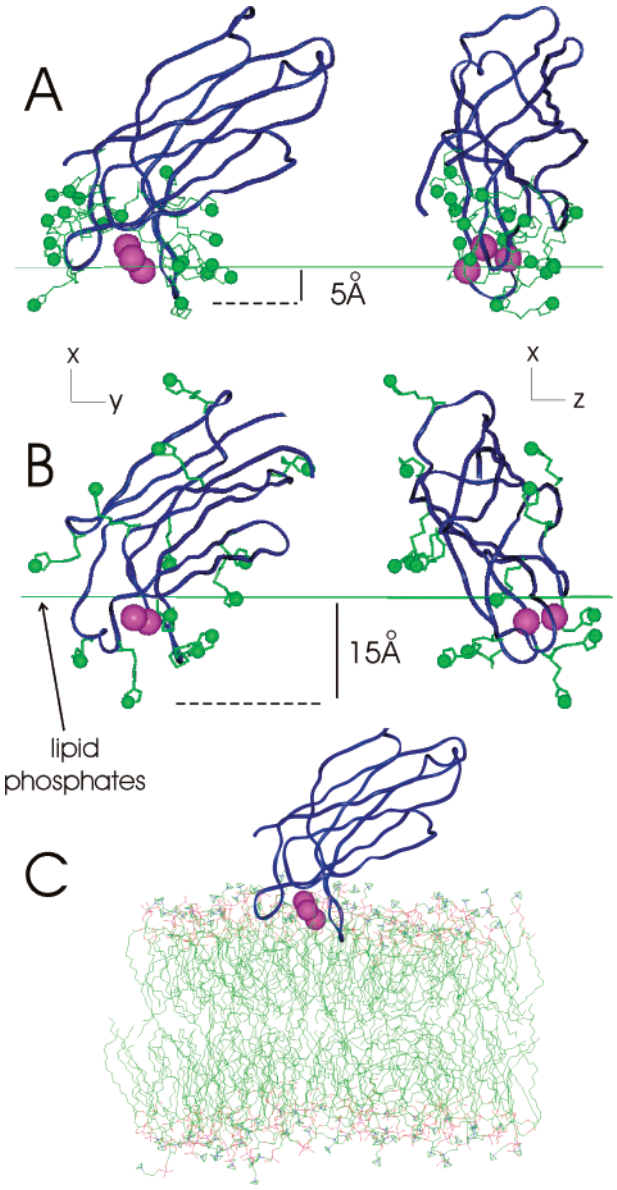

FIGURE 6: (A) Orientation and position of the solution structure of synaptotagmin I C2A on POPC:POPS bilayers (PDB code 1BYN). The R1 side chain and the nitrogen atom of the nitroxide radical for the 19 spin labeled mutants are shown in green. Calcium ions are shown in magenta. The horizontal green line represents the plane defined by the lipid phosphates. The best fit position corresponds to successive Euler angle rotations for the ϕ (*z*-axis), θ (x′-axis), and ψ (z′-axis) of 323°, 337°, and 160°, respectively, and a displacement of structure along the *x*-axis of −18.4 Å. These rotations and displacement are carried out using the center-of-mass of the protein on the local coordinate frame defined by the PDB file, where the bilayer phosphates lie in the *y*−*z* plane. Two views differing by a 90° rotation about the bilayer normal are shown. (B) Previously published position for the cPLA2 C2 domain (*28*). Two views differing by a 90° rotation about the bilayer normal are shown. (C) Backbone rendering of the synaptotagmin I C2A domain (PDB code 1BYN) docked to a dynamically simulated POPC bilayer (*53*−*55*). The bilayer simulation was performed in the absence of protein.

2 penetrate into the membrane as defined by the average position of the phosphates. All three calcium ions reside near the lipid phosphates. Two of the three Ca^{2+} ions lie a few Å on the aqueous side of the plane defined by the phosphates with the third Ca^{2+} site localized very close to the lipid phosphates. The β-sandwich region of the domain is tilted

from the $x-z$ plane so that strands 4 and 8 make angles of approximately 20° and 50° with respect to the membrane interface, respectively. In the other dimension, the β-sandwich region is roughly aligned along the $x-y$ plane. From the uncertainty in the experimental data, the side chain orientations and the fit, we believe that the uncertainty in the placement of the C2A along the bilayer normal is ±3 Å, and the uncertainty in the Euler angles defining its orientation is ±5°.

DISCUSSION

In the present work, site-directed spin labeling was used to generate a model for the orientation and depth of penetration of the synaptotagmin C2A domain when bound to membranes composed of POPC:POPS. This model is shown in Figure 6C along with a model for the lipid bilayer produced from an independent molecular dynamics simulation (*53*−*55*). The model indicates that side chains from both loops 1 and 3 of this domain penetrate the bilayer while residues from loop 2 reside on the aqueous side of the lipid phosphates. Of the three Ca^{2+}-binding loops, the backbones of loops 1 and 3 lie at or on the hydrocarbon side of the lipid phosphates, with the backbone of loop 3 penetrating approximately 5 Å below the level of the phosphates. Significantly, the three Ca^{2+} ions identified in the high-resolution NMR structure lie at or a few Å on the aqueous side of the lipid phosphates.

A comparison of the orientation for the synaptotagmin C2A domain with that obtained recently for the C2 domain from cPLA2 is shown in panels A and B, respectively, of Figure 6 (*28*). The orientations of the β-sheet regions of these two domains on the membrane interface are similar; however, compared to the synIC2A domain, which sites along the $x-y$ plane, the cPLA2 domain is tilted from the $x-y$ plane by about 30°. In addition, the cPLA2 C2 domain is more deeply buried in the bilayer by 5−7 Å. One R1 side chain in the cPLA2 C2 domain lies approximately 15 Å below the level of the lipid phosphates, whereas the deepest R1 side chain for synIC2A is inserted about 5−6 Å. In addition, the two Ca^{2+}-binding sites on the cPLA2 C2 domain lie below the level of the lipid phosphates, whereas the three Ca^{2+} ions on synIC2A lie near or on the aqueous side of the phosphates. Thus, the cPLA2 C2 domain experiences a higher degree of desolvation upon membrane binding than does synIC2A.

The differences seen in Figure 6 for these two domains are generally consistent with the expectations of electrostatic modeling (*37*). It has been proposed that the Ca^{2+}-dependent binding of C2 domains may occur by regulating long-range Coulombic interactions or by reducing the desolvation penalty for inserting the domain into the bilayer. Furthermore, recent electrostatic modeling indicates that the membrane binding of synIC2A should be regulated largely by long-range Coulombic interactions whereas the cPLA2 C2 domain binding should be regulated by desolvation (*37*). As a consequence, synIC2A should not reside as deeply in the bilayer as the cPLA2 C2 domain and indeed the data obtained here indicates that this is the case.

Interactions between proteins and the membrane interface that arise entirely from long-range Coulombic forces have been observed for certain model peptides or protein-derived peptides, such as pentalysine or the N-terminal end of src (*56*−*59*). In this case, these peptides reside several Å off the membrane interface, a position which is assumed because of the balance between a short-range desolvation energy and a long-range electrostatic attraction (*3*, *57*−*61*). Although long-range electrostatic interactions may be a major factor in determining the Ca^{2+}-dependent binding of synIC2A, the interaction of synIC2A is not purely electrostatic, and a number of residues within loops 1 and 3 make hydrophobic contact with the bilayer.

In addition to electrostatic and hydrophobic interactions, Ca^{2+} coordination appears to contribute to membrane binding. The third calcium ion that binds to synIC2A was shown previously to have only 5 coordinating ligands in solution (*36*, *62*), thus having an incomplete coordination sphere. It has been proposed that a phosphate from the lipid might be the sixth ligand, filling the coordination sphere around the third calcium ion in synIC2A (*62*). This coordination could account for the increased Ca^{2+} affinity that is observed upon membrane binding (*32*, *33*). The orientation obtained here for synIC2A (Figure 6A,C) places this third Ca^{2+} ion at the level of the lipid phosphates; thus, it is in an ideal position to interact with the lipid phosphates.

Previous work indicates that the structure of synIC2A is not altered in the presence of Ca^{2+} (*36*, *62*) but the domain appears to become stabilized. The EPR spectra at a number of loop sites are consistent with this result and indicate that there is a loss of motional averaging of the nitroxide spectrum upon Ca^{2+} binding (Figure 4). As indicated above (see Results), the decrease in motion appears to be due to a change in backbone motion and could result from a reduction in the amplitude of backbone fluctuations upon Ca^{2+} binding. Spectral changes also occur upon membrane binding for sites that are localized near or within the bilayer, and indicate that membrane binding is associated with a further loss of side chain or backbone motion. Thus, in addition to electrostatic interactions, the hydrophobic effect, and Ca^{2+} coordination, protein conformational entropy must make some contribution to the Ca^{2+}-dependent binding free energy of synIC2A.

The model presented here demonstrates the value of SDSL. This approach provides distance constraints between the bilayer surface and specific residues in synIC2A and allows both orientation and depth to be determined. SDSL is a sensitive technique, it is not limited by molecular weight, and it can be applied to a wide-range of membrane interacting domains. The data we obtain are consistent with other spectroscopic and biophysical characterizations of synIC2A but provide information that is not easily obtained using these other methods. For example, NMR chemical shift changes have been used to indicate the presence of lipid binding regions on synIC2A when bound to micelles. In particular, the NMR data suggest that membrane binding is localized primarily to loops 2 and 3 of the synIC2A domain (*24*). The results obtained here indicate that while the backbone of loop 2 is close to the bilayer, it does not actually penetrate below the level of the lipid phosphates. Instead, side chains from loop 1 appear to penetrate below the lipid phosphates. Fluorescence spectroscopy on site-directed tryptophan residues has been used to examine the membrane interaction of synIC2A (*31*). These data indicate that residues within the third Ca^{2+}-binding loop contact the bilayer, and the data place site 234 deeper in the bilayer than site 231. This result is

consistent with the data presented here, although the EPR data do not place spin labels at these sites as deep in the bilayer. Photoaffinity labeling with TID has been used to examine C2 domains, and the data show strong labeling of the cPLA2 C2 domain when membrane bound, indicating that it penetrates the bilayer and interacts hydrophobically. Only trace labeling of synIC2A by TID is found when this domain is bound to bilayers (*29*). Qualitatively, this result is consistent with the results obtained here, where the cPLA2 C2 domain is observed to penetrate more deeply into the bilayer than synIC2A. However, the placement of synIC2A shown in Figure 6A clearly indicates that this domain does interact hydrophobically with the bilayer and that its interaction includes more than an electrostatic component.

As indicated above, synaptotagmin plays a role in membrane fusion and apparently serves as the primary Ca^{2+} sensor for regulated exocytosis in neurons (*18*). There is evidence that synaptotagmin binds to proteins that form the SNARE complex; for example, synaptotagmin is reported to bind to the region on syntaxin that forms a link between the helical SNARE bundle and the transmembrane domain (*63*−*67*). Recent work indicates this portion of syntaxin is localized within the membrane-solution interface (*68*, *69*); thus, it is ideally positioned to interact with membrane-bound synaptotagmin. The binding of the C2A domain at the membrane interface may increase the effective local concentration of synaptotagmin near syntaxin thereby facilitating interactions between these proteins.

In summary, site-directed spin labeling has been used to examine the membrane orientation and penetration of the C2A domain from synaptotamin I. The data indicate that side chains from the first and third Ca^{2+}-binding loops penetrate below the level of the lipid phosphates with the backbone and side chains of the second Ca^{2+}-binding loop residing on the aqueous side of the membrane. Compared to the C2 domain from cPLA2, the synaptotagmin I C2A domain does not penetrate as deeply into the bilayer and its equilibrium position is translocated 5−7 Å toward the aqueous phase. This model is consistent with previous biophysical studies and computational work on these domains, and the results indicate that several forces, including electrostatic, hydrophobic, and entropic, contribute to the Ca^{2+}-dependent binding of these domains.

ACKNOWLEDGMENT

We thank Dr. Nathalie Cadiuex for assistance with the mutagenesis of synaptotagmin I C2A and Dr. Carl Creutz for the synaptotagmin construct. We also thank Dr. Carl Creutz and Dr. Gail Fanucci for many helpful discussions.

REFERENCES

1. Columbus, L., Kalai, T., Jeko, J., Hideg, K., and Hubbell, W. L. (2001) *Biochemistry 40*, 3828−3846.
2. McLaughlin, S., and Aderem, A. (1995) *TIBS 20*, 272−276.
3. Murray, D., Ben-Tal, N., Honig, B., and McLaughlin, S. (1997) *Structure 5*, 985−989.
4. Hurley, J. H., and Misra, S. (2000) *Annu. Revs. Biophys. Biomol. Struct. 29*, 49−79.
5. Gibson, T. J., Hyvonen, M., Musacchio, A., Saraste, M., and Birney, E. (1994) *Trends Biochem. Sci. 19*, 349−353.
6. Ponting, C. P., and Parker, P. J. (1996) *Protein Sci. 5*, 162−166.
7. Burd, C. G., and Emr, S. D. (1998) *Mol. Cell 2*, 157−162.
8. Gaullier, J.-M., Simonsen, A., D'Arrigo, A., Bremnes, B., Stenmark, H., and Aasland, R. (1998) *Nature 394*, 432−433.
9. Patki, V., Lawe, D. C., Corvera, S., Virbasius, J. V., and Chawla, A. (1998) *Nature 394*, 433−434.
10. Ponting, C. P. (1996) *Protein Sci. 5*, 2353−2357.
11. Kay, B. K., Yamabhal, M., Wendland, B., and Emr, S. D. (1999) *Protein Sci. 8*, 435−438.
12. Lemmon, M. A., Ferguson, K. M., O'Brien, R., Sigler, P. B., and Schlessinger, J. (1995) *Proc. Natl. Acad. Sci. U.S.A. 92*, 10472−10476.
13. Lemmon, M. A., Ferguson, K. M., and Abrams, C. S. (2002) *FEBS Lett. 513*, 71−76.
14. Lee, J. O., Yang, H., Georgescu, M. M., Di Cristofano, A., Maehama, T., Shi, Y., Dixon, J. E., Pandolfi, P., and Pavletich, N. P. (1999) *Cell 99*, 323−334.
15. Nalefski, E. A., and Falke, J. J. (1996) *Protein Sci. 5*, 2375−2390.
16. Nalefski, E. A., Wisner, M. A., Chen, J. Z., Sprang, S. R., Fukuda, M., Mikoshiba, K., and Falke, J. J. (2001) *Biochemistry 40*, 3089−3100.
17. Rizo, J., and Sudhof, T. C. (1998) *J. Biol. Chem. 273*, 15879−15882.
18. Tucker, W. C., and Chapman, E. R. (2002) *Biochem. J. 366*, 1−13.
19. Davletov, B. A., and Sudhof, T. C. (1993) *J. Biol. Chem. 268*, 26386−26390.
20. Zhang, X., Rizo, J., and Sudhof, T. C. (1998) *Biochemistry 37*, 12395−403.
21. Bai, J., Wang, P., and Chapman, E. R. (2002) *Proc. Natl. Acad. Sci. U.S.A. 99*, 1665−1670.
22. Mackler, J. M., Drummond, J. A., Loewen, C. A., Robinson, I. M., and Reist, N. E. (2002) *Nature*, 340−344.
23. Sutton, R. B., Davletoc, B. A., Berghuis, A. M., Sudhof, T. C., and Sprang, S. R. (1995) *Cell 80*, 929−938.
24. Chae, Y. K., Abildgaard, F., Chapman, E. R., and Markley, J. L. (1998) *J. Biol. Chem. 273*, 25659−63.
25. Xu, G.-Y., McDonagh, T., Yu, H.-A., Nalefski, E. A., Clark, J. D., and Cumming, D. A. (1998) *J. Mol. Biol. 280*, 485−500.
26. Nalefski, E. A., and Falke, J. J. (1998) *Biochemistry 37*, 17642−17650.
27. Ball, A., Nielsen, R., Gelb, M. H., and Robinson, B. H. (1999) *Proc. Natl. Acad. Sci. U.S.A. 96*, 6637−6642.
28. Frazier, A. A., Wisner, M. A., Malmberg, N. J., Victor, K. G., Fanucci, G. E., Nalefski, E. A., Falke, J. J., and Cafiso, D. S. (2002) *Biochemistry 41*, 6282−6292.
29. Davletov, B., Perisic, O., and Williams, R. L. (1998) *J. Biol. Chem. 273*, 19093−19096.
30. Bittova, L., Sumandea, M., and Cho, W. (1999) *J. Biol. Chem. 274*, 9665−9672.
31. Chapman, E. R., and Davis, A. F. (1998) *J. Biol. Chem. 273*, 13995-4001.
32. Fernandez, I., Arac, D., Ubach, J., Gerber, S. H., Shin, O., Gao, Y., Anderson, R. G., Sudhof, T. C., and Rizo, J. (2001) *Neuron 32*, 1057−1069.
33. Fernandez-Chacon, R., Konigstorfer, A., Gerber, S. H., Garcia, J., Matos, M. F., Stevens, C. F., Brose, N., Rizo, J., Rosenmund, C., and Sudhof, T. C. (2001) *Nature 410*, 41−49.
34. Swairjo, M. A., Concha, N. O., Kaetzel, M. A., Dedman, J. R., and Seaton, B. A. (1995) *Nat. Struct. Biol. 2*, 968−974.
35. Grobler, J. A., Essen, L.-O., Williams, R. L., and Hurley, J. H. (1996) *Nat. Struct. Biol. 3*, 788−795.
36. Shao, X., Fernandez, I., Sudhof, T. C., and Rizo, J. (1998) *Biochemistry 37*, 16106−15.
37. Murray, D., and Honig, B. (2002) *Mol. Cell 9*, 145−154.
38. Hubbell, W. L., Cafiso, D. S., and Altenbach, C. (2000) *Nat. Struct. Biol. 7*, 735−739.
39. Hubbell, W. L., Gross, A., Langen, R., and Lietzow, M. A. (1998) *Curr. Op. Struct. Biol. 8*, 649−656.
40. Hubbell, W. L., Mchaourab, H. S., Altenbach, C., and Lietzow, M. A. (1996) *Structure 4*, 779−783.
41. Hubbell, W., and Altenbach, C. (1994) *Curr. Opin. Struct. Biol. 4*, 566−578.
42. Altenbach, C., Greenhalgh, D. A., Khorana, H. G., and Hubbell, W. L. (1994) *Proc. Natl. Acad. Sci. U.S.A. 91*, 1667−1671.
43. Guan, K. L., and Dixon, J. E. (1991) *Anal. Biochem. 192*, 262−7.
44. Damer, C. K., and Creutz, C. E. (1994) *J. Biol. Chem. 49*, 31115−31123.
45. Sambrook, J., Fritsch, E. F., and Maniatis, T. (1989) *Molecular Cloning: A laboratory Manual*, Cold Spring Harbor Press, Plainview, NY.

46. Perin, M. S., Brose, N., Jahn, R., and Sudhof, T. C. (1991) *J. Biol. Chem. 266*, 623−9.
47. Hinderliter, A., Almeida, P. F. F., Creutz, C. E., and Biltonen, R. L. (2001) *Biochemistry 40*, 4181−4191.
48. Columbus, L., and Hubbell, W. L. (2002) *Trends Biochem. Sci. 27*, 288−295.
49. Langen, R., Oh, K. J., Cascio, D., and Hubbell, W. L. (2000) *Biochemistry 39*, 8396−8405.
50. Freed, J. H. (1976) in *Spin Labeling. Theory and Applications* (Berliner, L. J., Ed.) pp 592, Academic Press, New York.
51. Mchaourab, H., Lietzow, M., Hideg, K., and Hubbell, W. (1996) *Biochemistry 35*, 7692−7704.
52. Budil, D. E., Lee, S., Saxena, S., and Freed, J. H. (1996) *J. Magn. Reson. Ser. A 120*, 155−189.
53. Tieleman, D. P., Berendsen, H. J., and Sansom, M. S. (1999) *Biophys. J. 76*, 1757−69.
54. Tieleman, D. P., Berendsen, H. J., and Sansom, M. S. (1999) *Biophys. J. 76*, 3186−91.
55. Tieleman, D. P., Sansom, M. S., and Berendsen, H. J. (1999) *Biophys. J. 76*, 40−9.
56. Roux, M., Neumann, J.-M., Bloom, M., and Devaux, P. F. (1988) *Eur. Biophys. J. 16*, 267−273.
57. Ben-Tal, N., Honig, B., Peitzsch, R. M., Denisov, G., and McLaughlin, S. (1996) *Biophys. J. 71*, 561−575.
58. Victor, K., and Cafiso, D. S. (1998) *Biochemistry 37*, 3402−3410.
59. Victor, K. G., and Cafiso, D. S. (2001) *Biophys. J. 81*, 2241−2250.
60. Qin, Z., Wertz, S. L., Jacob, J., Savino, Y., and Cafiso, D. S. (1996) *Biochemistry 35*, 13272−13276.
61. Murray, D., Arbuzova, A., Hangyas-Mihalyne, G., Gambhir, A., Ben-Tal, N., Honig, B., and McLaughlin, S. (1999) *Biophys. J. 77*, 3176−3188.
62. Ubach, J., Zhang, X., Shao, X., Sudhof, T. C., and Rizo, J. (1998) *EMBO J. 17*, 3921−3930.
63. Bennett, M. K., Calakos, N., and Scheller, R. (1992) *Science 257*, 255−259.
64. Chapman, E. R., Hanson, P. I., An, S., and Jahn, R. (1995) *J. Biol. Chem. 270*, 23667−71.
65. Kee, Y., and Scheller, R. H. (1996) *J. Neurosci. 16*, 1975−1981.
66. Davis, A. F., Bai, J., Fasshauer, D., Wolowick, M. J., Lewis, J. L., and Chapman, E. R. (1999) *Neuron 24*, 363−376.
67. Lewis, J. L., Dong, M., Earles, C. A., and Chapman, E. R. (2001) *J. Biol. Chem. 276*, 15458−65.
68. Kim, C. S., Kweon, D.-H., and Shin, Y.-K. (2002) *Biochemistry 41*, 10928−10933.
69. Kweon, D. H., Kim, C. S., and Shin, Y. K. (2002) *Biochemistry. 41*, 9264−8.

BI0268145